

AFRL-ML-WP-TP-2006-447

**PARTIAL THERMODYNAMIC
PROPERTIES OF γ' -(Ni,Pt)₃Al IN THE
Ni-Al-Pt SYSTEM (PREPRINT)**



Evan Copland

FEBRUARY 2006

Approved for public release; distribution is unlimited.

STINFO COPY

This work, resulting in whole or in part from Department of the Air Force funding, has been submitted to the proceedings of the 2006 TMS Annual Meeting & Exhibition. If this work is published, TMS may assert copyright. The United States has for itself and others acting on its behalf an unlimited, paid-up, nonexclusive, irrevocable worldwide license to use, modify, reproduce, release, perform, display, or disclose the work by or on behalf of the Government. All other rights are reserved by the copyright owner.

**MATERIALS AND MANUFACTURING DIRECTORATE
AIR FORCE RESEARCH LABORATORY
AIR FORCE MATERIEL COMMAND
WRIGHT-PATTERSON AIR FORCE BASE, OH 45433-7750**

NOTICE AND SIGNATURE PAGE

Using Government drawings, specifications, or other data included in this document for any purpose other than Government procurement does not in any way obligate the U.S. Government. The fact that the Government formulated or supplied the drawings, specifications, or other data does not license the holder or any other person or corporation; or convey any rights or permission to manufacture, use, or sell any patented invention that may relate to them.

This report was cleared for public release by the Air Force Research Laboratory Wright Site (AFRL/WS) Public Affairs Office and is available to the general public, including foreign nationals. Copies may be obtained from the Defense Technical Information Center (DTIC) (<http://www.dtic.mil>).

AFRL-ML-WP-TP-2006-447 HAS BEEN REVIEWED AND IS APPROVED FOR PUBLICATION IN ACCORDANCE WITH ASSIGNED DISTRIBUTION STATEMENT.

**//Signature//*

PATRICK L. MARTIN

//Signature//

KENNETH E. DAVIDSON, Actg Chief
Metals Branch
Metals, Ceramics and NDE Division

//Signature//

GERALD J. PETRAK, Asst Chief
Metals, Ceramics and NDE Division
Materials and Manufacturing Directorate

This report is published in the interest of scientific and technical information exchange, and its publication does not constitute the Government's approval or disapproval of its ideas or findings.

Disseminated copies will show "//Signature//*" stamped or typed above the signature blocks.

REPORT DOCUMENTATION PAGE

Form Approved
OMB No. 0704-0188

The public reporting burden for this collection of information is estimated to average 1 hour per response, including the time for reviewing instructions, searching existing data sources, gathering and maintaining the data needed, and completing and reviewing the collection of information. Send comments regarding this burden estimate or any other aspect of this collection of information, including suggestions for reducing this burden, to Department of Defense, Washington Headquarters Services, Directorate for Information Operations and Reports (0704-0188), 1215 Jefferson Davis Highway, Suite 1204, Arlington, VA 22202-4302. Respondents should be aware that notwithstanding any other provision of law, no person shall be subject to any penalty for failing to comply with a collection of information if it does not display a currently valid OMB control number. **PLEASE DO NOT RETURN YOUR FORM TO THE ABOVE ADDRESS.**

1. REPORT DATE (DD-MM-YY) February 2006		2. REPORT TYPE Conference Paper Preprint		3. DATES COVERED (From - To)	
4. TITLE AND SUBTITLE PARTIAL THERMODYNAMIC PROPERTIES OF γ' -(Ni,Pt) ₃ Al IN THE Ni-Al-Pt SYSTEM (PREPRINT)				5a. CONTRACT NUMBER MIPR F4FBFN5097G001	
				5b. GRANT NUMBER	
				5c. PROGRAM ELEMENT NUMBER N/A	
6. AUTHOR(S) Evan Copland				5d. PROJECT NUMBER N/A	
				5e. TASK NUMBER N/A	
				5f. WORK UNIT NUMBER N/A	
7. PERFORMING ORGANIZATION NAME(S) AND ADDRESS(ES) Case Western Reserve University Cleveland, OH 44135				8. PERFORMING ORGANIZATION REPORT NUMBER	
9. SPONSORING/MONITORING AGENCY NAME(S) AND ADDRESS(ES) Materials and Manufacturing Directorate Air Force Research Laboratory Air Force Materiel Command Wright-Patterson AFB, OH 45433-7750				10. SPONSORING/MONITORING AGENCY ACRONYM(S) AFRL-ML-WP	
				11. SPONSORING/MONITORING AGENCY REPORT NUMBER(S) AFRL-ML-WP-TP-2006-447	
12. DISTRIBUTION/AVAILABILITY STATEMENT Approved for public release; distribution is unlimited.					
13. SUPPLEMENTARY NOTES This work, resulting in whole or in part from Department of the Air Force funding, has been submitted to the proceedings of the 2006 TMS Annual Meeting & Exhibition. If this work is published, TMS may assert copyright. This paper contains color. PAO Case Number: AFRL/WS 06-0482, 21 Feb 2006.					
14. ABSTRACT A series of measurements were made to determine how Pt influences the partial thermodynamic properties of Al and Ni in γ' -(Ni,Pt) ₃ Al and liquid in the Ni-Al-Pt system. The activities of Al and Ni were measured by the vapor pressure technique with a multiple effusion-cell vapor source coupled to a mass spectrometer (<i>multi-cell KEMS</i>). For a consistent $X_{Al} = 0.24$, adding Pt, from $X_{Pt} = 0.02$ to 0.25, reduces $a(Al)$ almost an order of magnitude, from about 2×10^{-4} to 2×10^{-5} , at 1560K. This occurred with a consistent $\Delta_m H(Al)$ of -203 ± 10 kJmol ⁻¹ and the decrease in $a(Al)$ was due to an increase in $\Delta_m S(Al)$, from -60 to -40 Jmol ⁻¹ K ⁻¹ with a decrease in the Ni/Pt ratio. The large negative $\Delta_m H(Al)$ and $\Delta_m S(Al)$ indicate Al-atoms are ordered in γ' -(Ni,Pt) ₃ Al. Nickel measurements showed $a(Ni)$ remains essentially constant, ~ 0.7 , indicating an increasingly positive ternary interaction between Ni-atoms and (Al + Pt)-atoms in γ' -(Ni,Pt) ₃ Al with Pt addition, where γ_{Ni} increased from about 0.7 to 1.2. This is supported by $\Delta_m H(Ni)$ in the range 6.1 to 7.1 ± 1.5 kJmol ⁻¹ at 1520K, and a positive $\Delta S_{xs}(Ni)_m$, and suggests disorder on the Ni-lattice. For a consistent $X_{Al} = 0.27$, adding Pt, from $X_{Pt} = 0.10$ to 0.25, also reduces $a(Al)$ but only by a factor of about 3, while $a(Ni)$ remained essentially constant, with γ_{Ni} increasing from about 0.7 to 0.95. A dramatic change in the mixing behavior was observed between the $X_{Al} = 0.24$ and 0.27 (hypo- and hyper-stoichiometric) series of alloys, where $\Delta_m H(Al)$ and $\Delta_m S(Al)$ are seen to increase about 50 kJmol ⁻¹ and 20 Jmol ⁻¹ K ⁻¹ at $T = 1566$ K, respectively. In contrast, $\Delta_m H(Ni)$ decreased about 16 kJmol ⁻¹ at $T = 1520$ K and $\Delta S_{xs}(Ni)_m$ changed from a positive to a negative value.					
15. SUBJECT TERMS					
16. SECURITY CLASSIFICATION OF:			17. LIMITATION OF ABSTRACT: SAR	18. NUMBER OF PAGES 30	19a. NAME OF RESPONSIBLE PERSON (Monitor) Patrick Martin 19b. TELEPHONE NUMBER (Include Area Code) N/A
a. REPORT Unclassified	b. ABSTRACT Unclassified	c. THIS PAGE Unclassified			

Partial Thermodynamic Properties of γ' -(Ni,Pt)₃Al in the Ni-Al-Pt system

Evan Copland
Case Western Reserve University, Cleveland, Ohio 44135

Abstract

A series of measurements were made to determine how Pt influences the partial thermodynamic properties of Al and Ni in γ' -(Ni,Pt)₃Al and liquid in the Ni-Al-Pt system. The activities of Al and Ni were measured by the vapor pressure technique with a multiple effusion-cell vapor source coupled to a mass spectrometer (*multi-cell KEMS*). For a consistent $X_{Al} = 0.24$, adding Pt, from $X_{Pt} = 0.02$ to 0.25, reduces $a(Al)$ almost an order of magnitude, from about 2×10^{-4} to 2×10^{-5} , at 1560K. This occurred with a consistent $\Delta_m \bar{H}(Al)$ of -203 ± 10 kJmol⁻¹ and the decrease in $a(Al)$ was due to an increase in $\Delta_m \bar{S}(Al)$, from -60 to -40 Jmol⁻¹K⁻¹ with a decrease in the Ni/Pt ratio. The large negative $\Delta_m \bar{H}(Al)$ and $\Delta_m \bar{S}(Al)$ indicate Al-atoms are ordered in γ' -(Ni,Pt)₃Al. Nickel measurements showed $a(Ni)$ remains essentially constant, ~ 0.7 , indicating an increasingly positive ternary interaction between Ni-atoms and (Al + Pt)-atoms in γ' -(Ni,Pt)₃Al with Pt addition, where γ_{Ni} increased from about 0.7 to 1.2. This is supported by $\Delta_m \bar{H}(Ni)$ in the range 6.1 to 7.1 ± 1.5 kJmol⁻¹ at 1520K, and a positive $\Delta_m \bar{S}^{xs}(Ni)$, and suggests disorder on the Ni-lattice. For a consistent $X_{Al} = 0.27$, adding Pt, from $X_{Pt} = 0.10$ to 0.25, also reduces $a(Al)$ but only by a factor of about 3, while $a(Ni)$ remained essentially constant, with γ_{Ni} increasing from about 0.7 to 0.95. A dramatic change in the mixing behavior was observed between the $X_{Al} = 0.24$ and 0.27 (hypo- and hyper-stoichiometric) series of alloys, where $\Delta_m \bar{H}(Al)$ and $\Delta_m \bar{S}(Al)$ are seen to increase about 50 kJmol⁻¹ and 20 Jmol⁻¹K⁻¹ at $T = 1566$ K, respectively. In contrast, $\Delta_m \bar{H}(Ni)$ decreased about 16 kJmol⁻¹ at $T = 1520$ K and $\Delta_m \bar{S}^{xs}(Ni)$ changed from a positive to a negative value.

1. Introduction

The Ni-Al-Pt system is currently receiving significant experimental interest, exemplified by the recent publication of new isothermal sections at $T = 1100$ and 1150°C (1373 and 1423K), measured transport kinetics and structural analysis [1-4]. This system is important to the oxidation protection of Ni-based superalloys used in gas-turbines applications, where Pt modified β -NiAl based coatings are currently used to ensure the formation of protective thermally grown α - Al_2O_3 -scales (TGO). The continual need to increase gas-turbine operating temperatures mean Ni-based superalloys now require the addition of a thermal barrier coating (TBC) on top of the aluminum rich coating and protective TGO [5]. The success of a TBC depends on the strength of the interfacial bond with the TGO scale and mechanical behavior of the scale. Therefore the objective of the aluminum rich coating has shifted from simply forming and maintaining a protective thermally grown α - Al_2O_3 -scale to providing a strongly adherent scale with significantly reduced susceptibility to cracking and spallation. The need for improved TGO scales is focusing research on understanding the detailed mechanisms of α - Al_2O_3 -scale formation on Pt modified aluminum-rich coatings. The scope of this research includes optimizing coating compositions for TGO scale properties, where both β and $\gamma' + \gamma$ coatings are being considered, and also the interaction of these coatings with Ni-based superalloy substrates [2, 6].

It is generally accepted that the addition of Pt improves the oxidation behavior of Ni-Al based alloys by promoting α - Al_2O_3 -scale formation and improving scale adhesion, however, the underlying mechanisms for “the Pt effect” remain unclear [5,7-10]. Most proposed mechanisms involve, to varying degrees, an increase in bond strength of the alloy / scale interface and a change in the multi-component diffusion behavior in the alloy, coating and TGO scale [11]. While interface strength is related to the thermodynamic properties of both the alloy and scale, this investigation is initially focused on improving our understanding of the multi-component diffusion behavior. As multi-component diffusion is a combination of multi-component solution thermodynamics and atomic mobility, a fundamental step is measuring the multi-component solution behavior. Specifically, determining how additions of Pt affect the partial thermodynamic properties (thermodynamic activities) of Al and Ni in β -(Ni,Pt)Al, γ' -(Ni,Pt)₃Al and γ -(Ni,Pt,Al) in the Ni-Al-Pt system. These activities were measured directly by the vapor pressure technique with a multiple effusion-cell vapor source coupled to a mass spectrometer (*multi-cell KEMS*) [12-17]. The partial thermodynamic properties of Pt were not considered in this publication because no Pt containing vapor species were measurable. A measurement procedure was developed for the Ni-Al-Pt system in an initial investigation of several β -(Ni,Pt)Al compositions [17]. The present publication will report a series of Al and Ni activity measurements made in eight γ' -(Ni,Pt)₃Al compositions and liquid of the same composition. Future publications will report measurements made in γ -(Ni,Pt,Al) and more detailed measurements in β -(Ni,Pt)Al as part of a more general investigation of the Ni-Al-Pt system.

2. Experimental

2.1 Alloys and Sample Preparation

The composition (in atomic percent) of the γ' -(Ni,Pt)₃Al alloys reported in this publication are listed in Table 1 and shown on the Ni-rich corner of the measured Ni-Al-Pt phase diagram at 1150°C (1423K), shown in Fig. 1 [1]. The alloys were divided into two groups: series A which is nominally $X_{Al} = 0.24$ and hypo-stoichiometric and series B which is nominally $X_{Al} = 0.27$ and hyper-stoichiometric, with respect to Al. All the alloys were supplied by Brian Gleeson's group at Iowa State University and were prepared by argon-arc melting the elements (at least 99.9 wt.% pure). After casting, each alloy was homogenized in a flowing argon gas atmosphere at $T = 1200^\circ\text{C}$ (1473K) for 6 hours and at $T = 1150^\circ\text{C}$ (1423K) for an additional 24 hours, water quenched and cut into 1 to 2mm thick slices. Directly prior to loading into the effusion cell (and pumping the *multi-cell KEMS* to 10^{-8} atms) the surface of each slice of alloy sample was removed by grinding with 600 grit SiC paper, roughly cut into cubes with a metal shear and ultrasonically cleaned in acetone then ethanol. Typically 0.7 to 1.5g of alloy sample were loaded into each effusion cell, enough to cover the base of the effusion-cell with approximately 2-3mm of sample, shown schematically in Fig. 2. Composition analyses of the alloys were performed by ICP (Inductively Coupled Plasma Spectroscopy) using the Varian Vista-Pro ICP-OES. For half the alloys their composition was measured before and after the activity measurement, in all cases both measured compositions agreed within the error.

TABLE 1

2.2 Activity Measurements

The partial thermodynamic properties (thermodynamic activities) of Al and Ni in these alloys were determined by the vapor pressure method by comparing the partial pressure of characteristic vapor species (Al(g) and Ni(g) in this case) in equilibrium with each alloy, $p(i)$, and a reference state, $p^\circ(i)$, according to Eq. 1 [18-20].

$$a(i) = \frac{p(i)}{p^\circ(i)} \quad (\text{Eq. 1})$$

The relative partial pressures of Al(g) and Ni(g) in equilibrium with the condensed samples were determined as a function of temperature by Knudsen effusion-cell mass spectrometry, *KEMS*. These measurements were made with a Nuclide/MAAS/PATCO 12-90-HT single focus 90° permanent sector mass spectrometer with an electron-multiplier detector. *KEMS* can be used to determine the relative partial pressures by sampling the flux of a species in a molecular beam (selected from the distribution of effusing molecules) coming from an effusion-cell by electron bombardment and subsequent formation of a representative ion beam that is sorted according to mass-to-charge ratio by common mass spectrometric

techniques. The partial pressure of a species inside the effusion-cell, $p(i)$, is directly proportional to the measured intensity of the representative ion beam, I_i , and absolute temperature, T ; Eq. 2 [12].

$$p(i) = \frac{I_i T}{S_i} \quad (\text{Eq. 2})$$

Where, S_i , is the instrument sensitivity factor which is a complex function of the: intersection of the molecular and electron beams, ion extraction efficiency, ionization cross-section, transmission probability of the mass analyzer, detection coefficient and isotopic abundance. The need for absolute partial pressures and therefore accurate instrument sensitivities is removed by using a furnace that is capable of containing 3 effusion-cells within the isothermal zone. This *multi-cell KEMS* configuration allows the direct comparison of the relative partial pressures of species in equilibrium with different condensed samples in adjacent effusion-cells at the same temperature. *Multi-cell KEMS* accounts for any variation in S_i between measurements within an experiment and between experiments. In theory, thermodynamic activities can be measured directly, by substituting Eq. 2 into Eq. 1, according to Eq. 3 [13-17].

$$a(i) = \frac{I_i}{I_i^{\circ}} \frac{g_{\text{ref}}}{g_{\text{alloy}}} \quad (\text{Eq. 3})$$

The temperature and all factors in S_i related to ionization and mass spectra analyses cancel, however, the geometric relationship between the molecular- and electron-beam remain, which is represented in Eq. (3) by, $g_{\text{ref}} / g_{\text{alloy}}$, the ‘geometry factor ratio’ (*GFR*). Provided all effusion-cells are isothermal and sampling of the molecular beam is independent of the vapor source, the *GFR* for a pair of cells only depends on the variation in the shape of the effusion orifices [16,17]. Consistent molecular beam sampling was achieved by inserting two fixed apertures (a “field aperture”, 0.8mm in diameter, and a “source aperture”, 2 mm in diameter about 38mm apart) between the effusion cell and ion source and accurate alignment of each effusion-cell orifice with the fixed apertures [14-17]. The apertures fix the shape and position of the molecular beam, which defines an ionization volume that is independent of the vapor source. This configuration works best when the fixed apertures define a source area for the molecular beam, A_s , that is smaller than the cross section of the effusion orifice, A_o , a condition referred to as “restricted collimation” [14-16]. The realization of this condition reduces the influence variations in effusion orifice shape have on the flux distribution of species in the molecular beam and *GFRs* are typically measured to be 1.00 ± 0.01 . Restricted collimation was achieved in this study with the field and source apertures listed above and the effusion-cells shown in Fig. 2.

The high vapor pressure of $\text{Al}(\text{g})$ and $\text{Al}_2\text{O}(\text{g})$ in equilibrium with the $\{\text{Al}(\text{l}) + \text{Al}_2\text{O}_3(\text{s})\}$ reference state precludes the routine use of the measurement procedure identified by Eq. 3 for the Ni-Al-Pt system. As a result an indirect measurement procedure using pure-Au(s,l) as a secondary reference was employed

in this study. In this method, activities are determined at each temperature, T , by comparing the ratio of the measured relative partial pressure of the characteristic vapor species in equilibrium with the alloy over $p^\circ(\text{Au})$ in equilibrium with pure-Au(s,l), $p(i) / p^\circ(\text{Au})$ or $I_i / I_{\text{Au}}^\circ$, to the ratio of $p^\circ(\text{Au})$ over the characteristic vapor species in equilibrium with the pure-element reference state $p^\circ(i)$, $p^\circ(\text{Au}) / p^\circ(i)$, as shown in Eq. 4.

$$a(i) = \frac{p(i)}{p^\circ(\text{Au})} \cdot \left[\frac{p^\circ(\text{Au})}{p^\circ(i)} \right] = \frac{I_i}{I_{\text{Au}}^\circ} \cdot \frac{S_{\text{Au}}}{S_i} \cdot \frac{g_{\text{ref}}}{g_{\text{alloy}}} \cdot \left[\frac{p^\circ(\text{Au})}{p^\circ(i)} \right] \quad (\text{Eq. 4})$$

The second term on the right hand side of Eq. 4, S_{Au} / S_i , is a calibration factor that relates the measured relative partial pressure of Au(g) in equilibrium with pure-Au(s,l), I_{Au}° , to the relative partial pressure of Al(g) and Ni(g) in equilibrium with the pure-element references, which are $\{\text{Al(l)} + \text{Al}_2\text{O}_3(\text{s})\}$ and $\{\text{Ni(s,l)} + \text{Al}_2\text{O}_3(\text{s})\}$, respectively. The calibration factors used in this study, $S_{\text{Au}} / S_{\text{Al}}$ and $S_{\text{Au}} / S_{\text{Ni}}$, were determined to be 0.154 ± 0.005 and 0.85 ± 0.03 , respectively and were independent of temperature. These could be considered to be “effective” ionization cross-section ratios, however a range of important variables were not adequately controlled, and they must be regarded as specific to the instrument used in this study. These values were determined in separate experiments with pure-Au(s,l) and the pure-element references in adjacent effusion-cells by comparing the measured ratio, $p^\circ(i) / p^\circ(\text{Au})$, to the tabulated ratio $[p^\circ(i) / p^\circ(\text{Au})]$, according to Eq. 5.

$$\frac{S_{\text{Au}}}{S_i} = \frac{I_{\text{Au}}^\circ}{I_i^\circ} \cdot \frac{g_i}{g_{\text{Au}}} \cdot \left[\frac{p^\circ(i)}{p^\circ(\text{Au})} \right] \quad (\text{Eq. 5})$$

The tabulated ratio $[p^\circ(\text{Au}) / p^\circ(i)]$ and $[p^\circ(i) / p^\circ(\text{Au})]$ used in Eq. 4 and Eq. 5 were determined at each measurement temperature with the “third law” treatment suggested by Paule *et. al.* [21] using the Gibbs free energy functions for the pure substances from reference [22] together with the measured “second law” reactions enthalpies listed in column 2 of Table 2. Repeated measurements of these reaction enthalpies were consistent and significantly different from the accepted values for $\{\text{Al(l)} + \text{Al}_2\text{O}_3(\text{s})\}$ [22,23], as a result the measured “second law” values were used in this study. This calculation procedure is different to that used in reference [17].

TABLE 2

It is important to note that the discrepancy shown in Table 2 mean the absolute partial pressure of Al(g) and Al₂O(g) in equilibrium with $\{\text{Al(l)} + \text{Al}_2\text{O}_3(\text{s})\}$ are not well known. While this has no influence on the accuracy of the measured activities reported in this study there is a need to better determine vaporization behavior of the Al-O system.

The indirect measurement procedure introduces some complications. The different shape of the ionization efficiency curves of Au(g), Al(g) and Ni(g) mean a consistent electron energy (25eV) must be used for all calibration and alloy activities measurements. Consistent electron energy was maintained by measuring the ionization potential of Au⁺ and Al⁺ in each experiment and setting the electron energy relative to these values. As the comparison between the measured and tabulated data is made at specific temperatures, accurate temperature measurement is critical. The temperature was measured with a pyrometer (*Mikron* M190V-TS) sighting a blackbody source (2.5 mm in diameter and 13.5 mm long) machined into the bottom of the effusion-cell and Mo-cell holder. The presence of pure-Au(s,l) as a secondary reference provides the primary temperature standard, the melting temperature of Au 1064.4°C (1337.5K), which was used to calibrate the pyrometer in each experiment and ensures accurate temperature measurement. In addition the enthalpy of the sublimation of pure-Au(s,l) is measured in every experiment, which provides a systematic method of checking the accuracy of the measured data. A vapor source capable of containing 3 effusion-cells allowed two alloys, together with the pure-Au(s,l) reference, to be measured in a single experiment. The steady state condition in each effusion-cell was verified at each temperature with repeat measurements 30–45 minutes apart. The typical variation in temperature and ion-intensity between repeat measurements was less than 0.5 K and 1 %, respectively. Typically measurements were made at a range of temperatures over three days and were taken in a “random” order to remove systematic errors.

3. Results

Figure 3 shows the experimental data from a typical activity measurement of alloys A2 (Ni-24.2Al-10.0Pt) and A4 (Ni-23.8Al-25.1Pt), plotted as the natural logarithm of the measured relative partial pressure, $\ln(I_i T)$, of Au(g), Ni(g) and Al(g) and Al₂O(g) versus inverse absolute temperature, $1/T$. The numbers on the Au(g) curve represent the order in which the measurements were made, each data point consists of 2 sets of 6 independent measurements taken 30 to 45 minutes apart. The reproducibility at each temperature indicates steady state while the linearity of the curves show the alloy compositions did not vary during the course of the experiment (in agreement with the measured compositions in Table 1) and that the instrument sensitivity was relatively consistent.

During the course of these experiments data was taken from both γ' -(Ni,Pt)₃Al and liquid phases for all alloy composition. The associated solid ↔ liquid phase transformations were made repeatedly in both directions and were completely reproducible for all alloys. The experimental data, as shown in Fig 3, for all measurements of γ' -(Ni,Pt)₃Al and liquid reported in this publication are summarized and listed in Table 3. This table contains the measured: temperature range; relative partial pressures of Al(g) as $\ln(I_{Al} T) = A + B/T$ and Ni(g) as $\ln(I_{Ni} T) = C + D/T$ for each composition; the “second-law” determination of partial enthalpies of sublimation for Al(g) and Ni(g), $\Delta_s \bar{H}(Al)$ and $\Delta_s \bar{H}(Ni)$, for each composition at the center

of the measured temperature range; enthalpy of sublimation for Au(g) from pure-Au(s,l) at 25°C (298K), $\Delta_s H^\circ(\text{Au})_{298}$, made during each experiment.

The activities of Al and Ni in γ' -(Ni,Pt)₃Al and liquid phases were calculated at each temperature by the method discussed in above (*i.e.*, Eq. (4) and Eq. (5) and the measured data in Table 2) and independent of the data summarized in Table 3. The measured activities are shown in Figs 4 to 7 as logarithmic plots of $a(\text{Al})$ and $a(\text{Ni})$ verses inverse absolute temperature, $1/T$, for the A and B series of alloys. These activities represent the partial mixing reaction of γ' -(Ni,Pt)₃Al and liquid from the pure elements. The partial enthalpy and entropy of mixing were determined from the measured temperature dependence of $a(\text{Al})$ and $a(\text{Ni})$, according to Eq. 6a, 6b and 6c.

$$\Delta_m \bar{G}(i) = RT \ln a(i) = \Delta_m \bar{H}(i) - T \Delta_m \bar{S}(i) \quad (\text{Eq 6a})$$

$$\Delta_m \bar{H}(i) = R \left[\frac{\partial \ln a(i)}{\partial (1/T)} \right]_P \quad (\text{Eq 6b})$$

$$\Delta_m \bar{S}(i) = -R \ln a(i) - RT \left[\frac{\partial \ln a(i)}{\partial T} \right]_P \quad (\text{Eq 6c})$$

The measured activities are summarized and listed in Table 4. The partial entropies of mixing are essentially constant over a small temperature range (a couple of hundred degrees) while the partial entropies of mixing are temperature dependent and the values listed in Table 4 are only valid for the center of the measured temperature range. The temperature dependence of the partial entropy of mixing for Al and Ni are shown in Fig. 8 and Fig. 9 for the A and B series of alloys, respectively.

TABLE 3

TABLE 4

Some information about the solid \leftrightarrow liquid phase transformations is obtained by looking at the sample surface after each measurement. All alloys exhibited clear evidence of dendritic growth with large regions of clean metal surface and some atomically flat steps, characteristic of vaporizing solid surfaces, as shown in Fig 10a for alloy B3. In addition there were regions with fine crystalline Al₂O₃ precipitates (identified by EDS analysis) on or just below the sample surface, as shown in Fig 10b. Presumably they are α -Al₂O₃ and they precipitated from the liquid on cooling and float to the surface. This suggests a significant increase in oxygen solubility in the liquid compared to γ' -(Ni,Pt)₃Al and that a small amount of Al₂O₃ dissolves and precipitates in the solid \leftrightarrow liquid phase transformation. This together with the discontinuities in activity plots shown in Figs 4 to 7 suggest the transformation behavior proposed in Table 5 within the identified temperature range. Alloys A1 to A4 are expected to melt congruently, while alloys B2 to B4

melt incongruently and alloy B1 melts with a eutectic reaction. Solid \leftrightarrow liquid phase transformations and their temperature were not the focus of this study and more accurate data could be obtained with a few changes in experiment procedure. The results related to the melting behavior of these alloys are important but will not be further discussed in this publication.

TABLE 5

4. Discussion

4.1 General Comments

The correct interpretation of thermodynamic property measurements relies on an accurate knowledge of the state of the system being studied (*i.e.*, absolute temperature, pressure, stable phases and phase compositions). Indeed the need to know phase composition as a function of temperature is the main reason single phase alloys were chosen for this study. For these measurements, however, the boundary of the system is defined by the inner surface of the effusion-cell and therefore the cell-material must be included in the equilibrium with the alloy samples [24,25]. Although our interest is in the Ni-Al-Pt system, the nature of the technique means the Ni-Al-Pt-O system is actually studied, specifically the $\{\gamma' + \text{Al}_2\text{O}_3 + \text{vapor}\}$ and $\{\text{liquid} + \text{Al}_2\text{O}_3 + \text{vapor}\}$ equilibria. Where γ' and liquid are saturated with O, and the Al_2O_3 is saturated with Al, Ni and Pt for the activities $a(\text{Al})$, $a(\text{Ni})$ and $a(\text{Pt})$ defined by alloy. Ni-Al-Pt-O is the ideal system to study with this technique because Al_2O_3 is in equilibrium with most alloy compositions, the O solubility in the solid and liquid alloy is low there should be no measurable influence on the activities of Al and Ni, the stoichiometry range of Al_2O_3 is small and it limits O transport through the effusion-cell wall. Figure 10b suggests O is more soluble in the liquid but quantifying this, as a function of temperature, is difficult and outside the scope of this study. So while the alloy phase compositions are not accurately known, in terms of O content, it is valid to apply these measured activities to the Ni-Al-Pt system, provided the actual state of the system is always kept in mind. The O solubility limit in γ' and the liquid can be added to these results when they become available.

The need to include the cell-material in the equilibrium is a restriction imposed on all effusion-cell studies [24]. This study differs in that the measurement procedure was developed and the reference states chosen to be consistent with this restriction [17]. The $\{\text{Ni}(\text{s,l}) + \text{Al}_2\text{O}_3(\text{s})\}$ reference state is convenient but not ideal as some Al must dissolve (at least 10^{-4} at. % Al at 1660K) before equilibrium is obtained with $\text{Al}_2\text{O}_3(\text{s})$. However, at this stage there appears to be no measurable difference between the vaporization behavior of Ni(g) from $\{\text{Ni}(\text{s,l}) + \text{Al}_2\text{O}_3(\text{s})\}$ and $\{\text{Ni}(\text{s,l}) + \text{NiAl}_2\text{O}_4(\text{s}) + \text{NiO}(\text{s})\}$, where $\{\text{Ni}(\text{s,l}) + \text{NiAl}_2\text{O}_4(\text{s}) + \text{NiO}(\text{s})\}$ is a better reference state. If this turns out to be incorrect these $a(\text{Ni})$ can be easily corrected by updating the $S_{\text{Al}} / S_{\text{Ni}}$ calibration factor used here. The $\{\text{Al}(\text{l}) + \text{Al}_2\text{O}_3(\text{s})\}$ reference state is both ideal and convenient as it provides the references, $p^\circ(\text{Al})$ and $p^\circ(\text{Al}_2\text{O})$ [17]. Provided both species

are measurable in the vapor in equilibrium with the alloy the activities of O and Al_2O_3 can be determined in addition to $a(\text{Al})$. These measurements are important because the {alloy + $\text{Al}_2\text{O}_3(\text{s})$ + vapor} equilibria represent the local equilibrium description of the alloy / scale interface observed during steady state oxidation [25]. Unfortunately $p(\text{Al}_2\text{O})$ was not measurable for all γ' alloys used in this study, therefore the results were not reported. However, from the limited results; $a(\text{Al}_2\text{O}_3)$ was very close to unity and apparently independent of alloy composition. Therefore $p(\text{O})$ or $p(\text{O}_2)$ depend directly on $a(\text{Al})$ in the alloy in accordance to the simplification typically used to determine the alloy / scale boundary condition [11].

The accuracy of these results was checked in each experiment with a “second-law” measurement of the enthalpy of the sublimation of $\text{Au}(\text{g})$ from pure- $\text{Au}(\text{s},\text{l})$, $\Delta_{\text{s}}\text{H}^\circ(\text{Au})_{298}$, which are shown in column 11 of Table 3. All values are within their experimental error and also agree with the value listed in Table 2 which were measured during the determination of the $S_{\text{Au}} / S_{\text{i}}$ calibration factors. This behavior is typical for both the *multi-cell KEMS* instrument and the measurement procedure used in this study and indicates the measured partial thermodynamic properties are accurate.

These results are discussed without directly considering the lattice structure of γ' -(Ni,Pt)₃Al or the liquid (inline with the phenomenological nature of the measurements). However, the measured phase boundaries in Fig. 1 show Ni and Al probably exist on different lattice-sites and Pt substitutes almost exclusively for Ni and there is a small range in Al composition either side of stoichiometry, $X_{\text{Al}} = 0.25$. The results for series A and B alloys will be discussed in turn.

4.2 Series A Alloys

Figure 4 shows that for a consistent Al concentration, $X_{\text{Al}} = 0.24$, increasing the Pt concentration from $X_{\text{Pt}} = 0.02$ to 0.25 in γ' -(Ni,Pt)₃Al and liquid, of the same composition, reduces $a(\text{Al})$ almost an order of magnitude. While $a(\text{Al})$ decreases in γ' -(Ni,Pt)₃Al with the decrease in Ni/Pt, the partial enthalpy of mixing of Al is consistent, $\Delta_{\text{m}}\bar{H}(\text{Al})$, at $-203 \pm 10 \text{ kJmol}^{-1}$. This behavior is consistent with the measured partial enthalpies of sublimation of $\text{Al}(\text{g})$ from alloys A1 through A4, listed in Table 3 and shown in Fig. 3 for A2 and A4. A consistent $\Delta_{\text{m}}\bar{H}(\text{Al})$ indicates the strength of the chemical bonding of Al-atoms in γ' -(Ni,Pt)₃Al is not influenced by a change in the Ni/Pt ratio. This suggests either, the chemical bond between Al–Ni atoms is almost identical to the bond between Al–Pt atoms or more simply that X_{Al} has the strongest influence on the bonding of Al-atoms in γ' -(Ni,Pt)₃Al. This first possibility needs to be checked by comparing the vaporization behavior of binary γ' -Ni₃Al and Pt₃Al. Either way the decrease in $a(\text{Al})$ appears to be due solely to the observed increase in partial entropy of mixing of Al, $\Delta_{\text{m}}\bar{S}(\text{Al})$, from -60 to $-40 \text{ Jmol}^{-1}\text{K}^{-1}$ at 1550K, with the decrease in Ni/Pt ratio, as shown in Fig. 8 and Table 4. The large negative values of $\Delta_{\text{m}}\bar{H}(\text{Al})$ and $\Delta_{\text{m}}\bar{S}(\text{Al})$ suggest Al-atoms are highly ordered in γ' -(Ni,Pt)₃Al and indicate a large negative non-configurational or excess contribution to the entropy of the Al-atoms. The

reason for the increase in $\Delta_m \bar{S}(\text{Al})$ is unclear but it suggests the entropy of the Al-lattice sites is influenced by changes in Ni/Pt ratio on the Ni-lattice because X_{Al} has remained essentially constant. An entropy based interaction between the Al-lattice and Ni-lattice. Clearly more work is need to relate these results to the lattice structure of $\gamma'-(\text{Ni,Pt})_3\text{Al}$ and better understand this behavior.

The liquid behaves in a similar manner to $\gamma'-(\text{Ni,Pt})_3\text{Al}$ but the decrease in $a(\text{Al})$ corresponds to a decrease in $\Delta_m \bar{H}(\text{Al})$ from -123 ± 5 to $-172 \pm 56 \text{ kJmol}^{-1}$. This indicates an increase in the binding of the Al-atoms in the liquid with the addition Pt which agrees with the decrease in $a(\text{Al})$. There is also a large negative excess contribution to the entropy of Al-atoms in the liquid and $\Delta_m \bar{S}(\text{Al})$ decreases from about -10 to $-25 \text{ Jmol}^{-1}\text{K}^{-1}$ (at about 1680K) with the addition of Pt. Both suggest significant ordering of the Al-atoms or cluster formation in the liquid that increases with the addition of Pt.

Figure 5 shows that while the concentration of Ni was reduced (from $X_{\text{Ni}} = 0.736$ to 0.511) with the addition of Pt ($X_{\text{Pt}} = 0.02$ to 0.251) in $\gamma'-(\text{Ni,Pt})_3\text{Al}$, the activity of Ni remained essentially constant (within the measurement error). This behavior indicates an increasingly positive ternary interaction between Ni-atoms and (Al + Pt)-atoms in $\gamma'-(\text{Ni,Pt})_3\text{Al}$ with Pt addition. This is clearly seen by re-plotting the $a(\text{Ni})$ data of alloys A1 through A4 in terms of the activity coefficient of Ni, where $\gamma_{\text{Ni}} = a(\text{Ni})/X_{\text{Ni}}$, (shown in Fig. 11a), where the measured γ_{Ni} increases from about 0.7 to 1.2. From Table 4, the measured partial enthalpies of mixing of Ni in these alloys are consistent and positive, within the range 6.1 to $7.1 \pm 1.5 \text{ kJmol}^{-1}$ at 1520K. This supports the existence of a positive ternary interaction between Ni-atoms and (Al + Pt)-atoms in $\gamma'-(\text{Ni,Pt})_3\text{Al}$ and also suggests consistent chemical bonding for Ni-atoms. Further, these results show a positive partial excess entropy of mixing for Ni, $\Delta_m \bar{S}^{\text{xs}}(\text{Ni})$, as listed in Table 4. The nature of the positive $\Delta_m \bar{S}^{\text{xs}}(\text{Ni})$ is unclear but it appears to be at odds with the large negative $\Delta_m \bar{S}^{\text{xs}}(\text{Al})$, *i.e.*, the high degree of ordering for Al-atoms is not matched by a corresponding ordering in the surrounding Ni-atoms. The $a(\text{Al})$ results suggested some type of entropy based interaction between the Al-lattice and Ni-lattice but there is no indication of this from the $a(\text{Ni})$ results. show no indication of this. Unfortunately there is no direct information about partial thermodynamic properties of Pt in $\gamma'-(\text{Ni,Pt})_3\text{Al}$ to help understand this behavior.

The behavior of Ni in liquid at compositions A1 through A4 is similar to $\gamma'-(\text{Ni,Pt})_3\text{Al}$. The activity of Ni remained essentially constant as the concentration of Ni was reduced with the addition of Pt. Again this results from an increasingly positive ternary interaction between Ni-atoms and (Al + Pt)-atoms with Pt addition, as shown in Fig. 11a. This is accompanied with an increase in both the partial enthalpy and entropy of mixing of Ni in the liquid. It is important to note that for both $\gamma'-(\text{Ni,Pt})_3\text{Al}$ and liquid the interactions in both binaries, Ni-Al and Ni-Pt, are negative (*i.e.*, $\gamma_{\text{Ni}} < 1$) with the Ni-Al interaction stronger than Ni-Pt. As a result the behavior seen here must be a ternary interaction between Ni-atoms and (Al + Pt)-atoms.

4.3 Series B Alloys

Initially the most striking result from the B series of alloys (Fig. 6 and Fig. 7) is the inconsistent behavior of alloy B1. This alloy exhibits a small $\Delta_m \bar{H}(\text{Al})$ ($-88.2 \pm 3.9 \text{ kJmol}^{-1}$) and a large $\Delta_m \bar{H}(\text{Ni})$ ($-39.5 \pm 3.0 \text{ kJmol}^{-1}$) compared to all other alloys measured in this study. In addition the melting behavior of this alloy is characterized by a large discontinuity in the temperature dependence of $p(\text{Al})$ and $p(\text{Ni})$ that is not seen with the other alloys. This behavior is due to B1 being a two phase, $\gamma' + \beta$, alloy and there are significant changes in phase composition with temperature. The changes in phase composition dominate the vaporization behavior of B1 and therefore the temperature dependence of $a(\text{Al})$ and $a(\text{Ni})$ does not give any information about the mixing behavior of either γ' or β . Without accurate phase composition data these results cannot be used to discuss the solution behavior of $\gamma'-(\text{Ni,Pt})_3\text{Al}$.

For alloys B2, B3 and B4, Fig. 6 shows that for a consistent Al concentration, $X_{\text{Al}} = 0.27$, increasing the Pt concentration from $X_{\text{Pt}} = 0.10$ to 0.25 in $\gamma'-(\text{Ni,Pt})_3\text{Al}$ and liquid, of the same composition, reduces $a(\text{Al})$ by about a factor of about 3. In line with the small increase in X_{Al} the $a(\text{Al})$ in these alloys is higher than in the A series of alloys. For these alloys the $\Delta_m \bar{H}(\text{Al})$ is relatively independent of the decrease in Ni/Pt ratio, and was measured in the range, -146.4 ± 6.8 to $-163 \pm 12 \text{ kJmol}^{-1}$ but it is not as obvious as seen for A series of alloys. The critical point, however, is that a small change in X_{Al} from 0.24 to 0.27 (from hypo- to hyper-stoichiometric) has a dramatic influence on the mixing behavior and therefore the chemical bonding of Al-atoms in $\gamma'-(\text{Ni,Pt})_3\text{Al}$; where $\Delta_m \bar{H}(\text{Al})$ increases about 50 kJmol^{-1} at $T = 1566\text{K}$. These results also suggest almost identical chemical bonds between Al-Ni and Al-Pt atoms and support the idea that X_{Al} has the strongest influence on the bonding of Al-atoms in $\gamma'-(\text{Ni,Pt})_3\text{Al}$. A large negative excess contribution to the entropy of the Al-atoms is also present in these alloys but the decrease in $a(\text{Al})$ with Pt addition is not clearly due to an increase in the partial entropy of mixing of Al, $\Delta_m \bar{S}(\text{Al})$, Fig. 9 and Table 4. Again there is a dramatic change in $\Delta_m \bar{S}(\text{Al})$ going from hypo- to hyper-stoichiometry in $\gamma'-(\text{Ni,Pt})_3\text{Al}$ where $\Delta_m \bar{S}(\text{Al})$ increases about $20 \text{ Jmol}^{-1}\text{K}^{-1}$ at $T = 1566\text{K}$. These results suggest $\gamma'-(\text{Ni,Pt})_3\text{Al}$ remains highly ordered, with respect to Al-atoms, but the lattice structure must change significantly at $X_{\text{Al}} = 0.25$.

The solution behavior of the liquid, in terms of both Al and Ni, observed for series B alloys is similar to that observed for series A alloys. The $a(\text{Al})$ decreased with the addition Pt or decreasing Ni/Pt ratio. A similar negative non-configurational contribution to the entropy of the Al-atoms is observed suggesting ordering of the Al-atoms in the liquid. The $a(\text{Ni})$ remained essentially constant as the concentration of Ni was reduced with the addition of Pt. The consistent positive partial enthalpy and entropies of mixing for Ni were observed for all compositions (apart from B1), again suggesting an increasingly positive ternary interaction between Ni-atoms and (Al + Pt)-atoms with Pt addition.

Figure 7 shows that while the concentration of Ni was reduced (from $X_{\text{Ni}} = 0.638$ to 0.481) with the addition of Pt ($X_{\text{Pt}} = 0.10$ to 0.252) in $\gamma'-(\text{Ni,Pt})_3\text{Al}$, the activity of Ni remained essentially constant (within

the measurement error). Again indicating an increasing but negative ternary interaction between Ni-atoms and (Al + Pt)-atoms in γ' -(Ni,Pt)₃Al with Pt addition (shown in Fig. 11b) where γ_{Ni} increases from 0.7 to 0.95. The increase in X_{Al} going from series A to series B alloys corresponds to a general decrease in $a(\text{Ni})$ from 0.65 to 0.45 in γ' -(Ni,Pt)₃Al. From Table 4, the measured $\Delta_{\text{m}}\bar{H}(\text{Ni})$ in series B alloys is relatively consistent at -7.8 to -10.5 ± 2.0 kJmol⁻¹ at 1520K. As seen with Al, there is a dramatic change in the mixing behavior of Ni and hence the chemical bonding of Ni-atoms in γ' -(Ni,Pt)₃Al between series A and series B alloys. In this case, $\Delta_{\text{m}}\bar{H}(\text{Ni})$ decreases about 16 kJmol⁻¹ at $T = 1520\text{K}$ and $\Delta_{\text{m}}\bar{S}^{\text{xs}}(\text{Ni})$ changes from a positive to a negative value. The decrease in both $\Delta_{\text{m}}\bar{H}(\text{Ni})$ and $\Delta_{\text{m}}\bar{S}^{\text{xs}}(\text{Ni})$ indicate an increase in the degree of ordering for Ni-atoms on the hyper- side relative to the hypo-stoichiometric side of γ' -(Ni,Pt)₃Al.

5. Conclusion

For the hypo-stoichiometric alloys, series A, adding Pt to γ' -(Ni,Pt)₃Al reduces $a(\text{Al})$ almost an order of magnitude. This occurred with a consistent $\Delta_{\text{m}}\bar{H}(\text{Al})$ and suggests either, the chemical bond between Al–Ni atoms and Al–Pt atoms is almost identical or more simply X_{Al} has the strongest influence on the bonding of Al-atoms in γ' -(Ni,Pt)₃Al. The decrease in $a(\text{Al})$ is due to an increase in the large negative $\Delta_{\text{m}}\bar{S}(\text{Al})$ with decreasing Ni/Pt ratio. The large negative $\Delta_{\text{m}}\bar{H}(\text{Al})$ and $\Delta_{\text{m}}\bar{S}(\text{Al})$ indicate Al-atoms are highly ordered in γ' -(Ni,Pt)₃Al. The reason for the increase in Al entropy with Ni/Pt ratio is not understood but the result implies an entropy-based interaction between the Al-lattice and the Ni-lattice.

The Ni measurements for series A alloys showed that while X_{Ni} was reduced with the addition of Pt the activity of Ni remains essentially constant. This behavior indicates an increasingly positive ternary interaction between Ni-atoms and (Al + Pt)-atoms in γ' -(Ni,Pt)₃Al with Pt addition. This was supported by positive $\Delta_{\text{m}}\bar{H}(\text{Ni})$ and a positive $\Delta_{\text{m}}\bar{S}^{\text{xs}}(\text{Ni})$ that suggest the Ni-lattice is disordered. This appears to be at odds with the ordering on the Al-lattice and the indication of an entropy based interaction between the two lattices.

For the hyper-stoichiometric alloys, series B, adding Pt to γ' -(Ni,Pt)₃Al reduced $a(\text{Al})$ by about a factor of 3. This also occurred with a consistent $\Delta_{\text{m}}\bar{H}(\text{Al})$ that was relatively independent of Ni/Pt ratio. The critical point, however, is that there is a dramatic change in the mixing behavior between $X_{\text{Al}} = 0.24$ and 0.27 (*i.e.*, hypo- to hyper-stoichiometric composition of γ' -(Ni,Pt)₃Al) where $\Delta_{\text{m}}\bar{H}(\text{Al})$ and $\Delta_{\text{m}}\bar{S}(\text{Al})$ increase about 50 kJmol⁻¹ and 20 Jmol⁻¹K⁻¹ at $T = 1566\text{K}$, respectively. This supports the observation that X_{Al} has the strongest influence on the bonding of Al-atoms in γ' -(Ni,Pt)₃Al. The large negative excess contribution to the entropy of the Al-atoms indicate γ' -(Ni,Pt)₃Al remains highly ordered for Al.

The Ni measurements for series B alloys also showed an increasing ternary interaction between Ni-atoms and (Al + Pt)-atoms in γ' -(Ni,Pt)₃Al with Pt addition. The increase in X_{Al} from series A alloys decreased $a(Ni)$. The measured $\Delta_m \bar{H}(Ni)$ in these alloys were relative consistent but negative and indicate a similarly dramatic change in the mixing behavior of Ni in γ' -(Ni,Pt)₃Al between series A and series B alloys. The measured $\Delta_m \bar{H}(Ni)$ decreased about 16 kJmol⁻¹ at $T = 1520K$ and $\Delta_m \bar{S}^{xs}(Ni)$ changed from a positive to a negative value. Both indicate an increase in the degree of ordering for Ni-atoms in hyper-stoichiometric γ' -(Ni,Pt)₃Al.

Measurements made in the liquid showed similar behavior to γ' -(Ni,Pt)₃Al for Al and Ni in both series A and series B alloys. $a(Al)$ decreased with the addition of Pt and was accompanied by a decrease in $\Delta_m \bar{H}(Al)$ and a negative excess contribution to $\Delta_m \bar{S}(Al)$. Both properties indicate an increase in the binding of the Al-atoms with Pt addition and significant ordering of the Al-atoms in the liquid. $a(Ni)$ remained essentially constant in the liquid, again suggesting an increasingly positive ternary interaction between Ni-atoms and (Al + Pt)-atoms with Pt addition.

Clearly more work is need to relate these measurements to the lattice structure of γ' -(Ni,Pt)₃Al to better understand the solution behavior, particularly the dramatic change in the mixing behavior when going from hypo- to hyper-stoichiometry compositions of γ' -(Ni,Pt)₃Al, in terms of Al content. Unfortunately there are no direct measurements of the partial thermodynamic properties of Pt in γ' -(Ni,Pt)₃Al or alternatively integral mixing enthalpies of ternary compositions in γ' -(Ni,Pt)₃Al determined by high temperature reaction calorimetry [26]. This information will provide a more complete picture of the solution behavior of γ' -(Ni,Pt)₃Al and help answer some of the issues raised with these results.

Acknowledgements

The help of Pat Martin and Brian Gleeson for providing this research opportunity and the alloys considered in this study is gratefully acknowledged. The funding for this work came from AFRL / MLLM, Materials for Air Breathing Propulsion Project and NASA Glenn Research Centre's Low Emission Alternative Power Project.

6. References

1. S. Hayashi, S. Ford, D. Young, D. Sordelet, M. Besser, B. Gleeson, α -NiPt(Al) and phase equilibria in the Ni-Al-Pt system at 1150°C, *Acta Materialia*, 53, 2005, 3319.
2. B. Gleeson, W. Wang, S. Hayashi, D. Sordelet, Effects of Platinum on the Interdiffusion and Oxidation Behavior of Ni-Al-Based Alloys, *Mater Sci Forum*, 461-462, 2004, 213.

3. H. Meininger, M. Ellner, Phase transformations and the type of lattice distortion of some platinum-rich phases belonging to the Cu family, *Journal of Alloys and Compounds*, 353, 2003, 207.
4. J. Kamm, W. Milligan, Phase stability in (Ni, Pt)₃Al alloys, *Scripta Metall Mater*, 31, 1994, 1461.
5. J. Nicholls, Advances in Coating Design for High-Performance Gas Turbines, *Materials Research Society Bulletin*, 28(9), 2003, 659.
6. S. Hayashi, W. Wang, D. Sordelet, B. Gleeson, Interdiffusion Behavior of Pt Modified γ -Ni + γ' -Ni₃Al Alloys Coupled to Ni-Al based Alloys, *Metallurgical and Metal Transactions A*, 36A, July, 2005, 1769.
7. C. Corti, D. Coupland, G. Selman, Platinum-Enhanced Superalloys, *Platinum Metals Review*, 24(1), 1980, 2.
8. G. Tatlock, T. Hurd, J. Punni, High Temperature Degradation of Nickel Based Alloys: A Consideration of the Role of Platinum, *Platinum Metals Review*, 31(1), 1987, 26.
9. J. Fountain, F. Golightly, F. Stott, G. Wood, The Influence of Platinum on the Maintenance of α -Al₂O₃ as a Protective Scale, *Oxidation of Metals*, 10(5), 1976, 341.
10. V. Tolpygo, D. Clarke, K. Murphy, Oxidation-induced failure of EB-PVD thermal barrier coatings, *Surface and Coatings Technology*, 146-147, 2001, 124.
11. P. Kofstad, High Temperature Corrosion, Elsevier, New York, 1988.
12. M. Inghram, J. Drowart, Mass Spectrometry Applied to High Temperature Chemistry, *High Temperature Technology*, Oct 6-9, 1959, 338.
13. A. Büchler, J. Stauffer, in Thermodynamics (IAEA Vienna, 1966) vol. 1, 271.
14. C. Chatillion, C. Senillou, M. Allibert, A. Pattoret, *Rev. Sci. Instrum.* 47(3), 1976, 334.
15. P. Morland, C. Chatillion, P. Rocabois, *High Temp. and Materials Sci.* 37, 1997, 167.
16. C. Chatillion, L. Malheiros, P. Rocabois, M. Jeymond, *High Temp. High Pressures*, 34, 2002, 213.
17. E. Copland, Thermodynamic Effect of Platinum Addition to β -NiAl: An Initial Investigation, NASA/CR-2005213330, NASA, Cleveland, OH, 2005.
18. G. N. Lewis, M. Randall, Thermodynamics (revised by K. S. Pitzer and L. Brewer) McGraw-Hill, New-York, 1961.
19. C. H. P. Lupis, Chemical Thermodynamics of Materials, North-Holland, New-York, 1983.
20. O. Kubaschewski, C. B. Alcock, Metallurgical Thermochemistry, (6th Edition) Pergamon Press, Oxford, 1979.
21. R. C. Paule, J. Mandel, Analysis of Interlaboratory Measurements on the Vapor Pressure of Gold, SRM 745, National Bureau of Standards Special Publication 260-19, (1970). Also published in *Pure and Applied Chem.* 31, 1972, 371.
22. L. V. Gurvich, I. V. Veyts, C. B. Alcock, Thermodynamic Properties of Individual Substances, English Version, Begell House, 1996.
23. M. W. Chase, NIST-JANAF Thermochemical Tables, 4th Ed., American Chemical Society, 1998.
24. C. Chatillon, M. Allibert, Thermodynamic and Physico-Chemical Behavior of the Interactions Between Knudsen Effusion-cells and the Systems Under Investigation, *NBS Special Publication 561, 10th Materials Research Symposium on Characterization of High Temperature Vapors and Gases*, Sept. 18-22, 1978, 181.
25. E. Copland, Measuring the Thermodynamics of the Alloy/Scale Interface, in E. Opila, J. Fergus, T. Maruyama, J. Mizusaki, T. Narita, D. Shifler and E. Wuchina, eds., *High Temperature Corrosion and Materials Chemistry, V*, The Electrochemical Society, 2004.
26. Hsin-Ning Su and Philip Nash, Enthalpies of formation in the Al-Ni-Ru system by direct reaction synthesis calorimetry, *Journal of Alloys and Compounds*, 403(1-2), 2005, 217-222.

Tables

Table 1. Measured Alloy Composition (at. %)

Alloy	Ni	Al	Pt	Ni/Pt	Al/Pt
A1	73.6	24.3	2.0	35.05	11.57
A2	65.8	24.2	10.0	6.58	2.42
A3	57.9	24.0	18.1	3.2	1.33
A4	51.1	23.8	25.1	2.04	0.95
B1	70.8	27.2	2.0	35.4	13.6
B2	63.8	26.4	9.8	6.51	2.69
B3	54.9	27.0	18.1	3.03	1.49
B4	48.1	26.7	25.2	1.91	1.06

experimental error $\pm 0.5\text{at}\%$

Table 2. Reaction Enthalpies at 25°C (298K) for Au(g), Ni(g), Al(g) and Al₂O(g);
Measured “Second-Law” Values and Accepted Values

Reaction	Measured (kJmol ⁻¹)	IVTAN [22] (kJmol ⁻¹)	JANAF [23] (kJmol ⁻¹)
Au(s,l) = Au(g)	363.5±2.8 367.0±1.3*		367.0±0.9 [21]
Ni(s) = Ni(g)	428.3±2.6	428.0±8.0	430.1±8.4
Al(s) = Al(g)	341.0±2.2	330.0±3.0	329.7±4.2
4/3Al(s) + 1/3Al ₂ O ₃ (s) = Al ₂ O(g)	414.2±3.6	409.9±55	413.4±50
4/3Al(g) + 1/3Al ₂ O ₃ (s) = Al ₂ O(g)	-41.1±3.2	-30.0±4.3	-26.2±3.0
2Al(g) + O(g) = Al ₂ O(g)	-1075.5±9.0	-1057.8±20.0	-1053.7±150

* 3rd law measurement

Table 3. Summary of all Measured Experimental Data of γ' -(Ni,Pt)₃Al and Liquid.

Alloy		T range (K)	$\ln(I_{Al}T) = A + B/T$		$\Delta_S \bar{H}(Al)$ (kJmol ⁻¹)	T range (K)	$\ln(I_{Ni}T) = C + D/T$		$\Delta_S \bar{H}(Ni)$ (kJmol ⁻¹)	$\Delta_S H^\circ(Au)_{298}$ (kJmol ⁻¹)
			A	-Bx10 ⁻³			C	-Dx10 ⁻³		
A1	γ'	1530-1620	53.6±0.3	63.7±0.4	530±3	1425-1620	46.7±0.2	49.5±0.3	411±2	362.7±2.0
	L	1651-1690	46.9±0.5	52.6±0.9	438±7	1651-1690	46.0±0.4	48.3±0.6	402±5	
A3	γ'	1530-1620	52.3±0.8	63.4±1.2	527±10	1425-1620	46.7±0.7	49.2±1.0	410±8	362.7±2.0
	L	1651-1690	47.1±0.3	54.8±0.5	456±4	1651-1690	46.0±0.5	48.2±0.8	401±6	
A2	γ'	1500-1623	52.6±0.6	62.9±0.8	523.7±7.2	1400-1623	46.7±0.1	49.4±0.2	411±2	363.1±1.0
	L	1653-1680	49.4±3.8	57.6±6.4	479±53	1653-1680	46.9±0.5	49.7±0.8	413±7	
A4	γ'	1550-1623	50.9±0.8	62.4±1.3	519±11	1400-1623	46.7±0.1	49.5±0.2	411.3±1.2	363.1±1.0
	L	1652-1680	48.7±3.6	58.5±6.1	486±50	1652-1680	46.2±1.4	48.6±2.4	405±20	
B1	γ'	1450-1637	44.1±0.4	48.9±0.6	406.6±4.6	1450-1637	49.4±0.4	55.0±0.6	457.0±5.0	362.2±1.0
	L	1637-1708	47.1±0.3	53.2±0.5	442.6±4.4	1637-1708	45.8±0.4	49.2±0.8	408.8±6.6	
B3	γ'	1500-1624	48.4±1.5	57.0±2.3	474±19	1450-1624	47.5±0.4	52.0±0.6	432.3±5.4	362.2±1.0
	L	1637-1708	46.7±0.4	54.3±0.6	451.4±5.1	1637-1708	47.4±0.5	51.8±0.8	431.0±6.6	
B2	γ'	1483-1620	47.7±0.6	55.1±0.9	458.6±0.9	1389-1620	47.4±0.1	51.7±0.2	429.6±1.4	362.0±1.2
	L	1647-1720	47.6±2.2	55.0±3.4	457±28	1647-1720	45.5±0.5	48.6±0.9	404±7.2	
B4	γ'	1500-1620	47.9±1.0	57.1±1.5	475±13	1389-1620	47.1±0.1	51.3±0.2	426.8±1.1	362.0±1.2
	L	1647-1720	46.8±0.4	55.6±0.7	462.5±5.6	1647-1720	45.4±0.3	48.6±0.5	404.3±4.5	
B2	γ'	1487-1610	49.0±1.3	57.2±2.1	476±17	1487-1610	47.3±0.3	51.6±0.4	429.3±3.7	362.3±1.2
	L	1635-1750	46.4±0.3	53.1±0.5	441.9±4.2	1635-1750	45.0±0.2	47.9±0.3	398.3±2.6	
A3	γ'	1538-1610	52.6±0.8	65.2±1.2	542±10	1424-1610	46.4±0.2	50.0±0.2	415.4±2.0	362.3±1.2
	L	1635-1750	46.2±0.4	54.5±0.7	453.3±5.4	1635-1750	45.0±0.3	47.7±0.4	396.3±3.7	
A2	γ'	1518-1627	51.6±1.6	62.2±2.5	517±21	1426-1627	46.4±0.2	49.5±0.3	411.4±2.4	362.7±1.2
	L	1656-1742	45.8±0.4	52.8±0.7	438.6±6.0	1656-1742	44.7±0.3	47.1±0.5	391.7±4.0	
B3	γ'	1518-1627	47.9±1.3	56.2±2.0	467±17	1426-1627	47.0±0.4	51.3±0.6	426.3±4.7	362.7±1.2
	L	1656-1742	45.6±0.2	52.5±0.4	436.3±2.9	1656-1742	47.1±0.4	51.4±0.6	427.2±5.0	

Table 4. Partial Enthalpies and Entropies of Mixing for Ni and Al in γ' -(Ni,Pt)₃Al and Liquid

Alloy		$\Delta_m \bar{H}(Al)$ (kJmol ⁻¹)	$\Delta_m \bar{S}(Al)$ (Jmol ⁻¹ K ⁻¹)	$\Delta_m \bar{S}^{xs}(Al)$ (Jmol ⁻¹ K ⁻¹)	T (K)	$\Delta_m \bar{H}(Ni)$ (kJ/mol)	$\Delta_m \bar{S}(Ni)$ (Jmol ⁻¹ K ⁻¹)	$\Delta_m \bar{S}^{xs}(Ni)$ (Jmol ⁻¹ K ⁻¹)	T (K)
A1	γ'	-200.5±5.8 ₈	-56.8±3.7	-68.6±3.7	1575	7.1±1.3 ₁₂	9.3±0.8	6.8±0.8	1522
	L	-123.1±5.4 ₄	-9.7±3.2	-21.4±3.2	1670	11.9±5.0 ₄	12.0±3.0	9.4±3.0	1670
A2	γ'	-201.9±8.0 ₂₄	-53.2±5.2	-65.0±5.2	1564	6.7±1.2 ₃₈	8.4±0.8	4.9±0.8	1512
	L	-137.9±7.8 ₉	-14.4±4.7	-26.2±4.7	1697	2.3±6.1 ₉	6.0±3.6	2.5±3.6	1697
A3	γ'	-207.8±25 ₁₃	-51.2±16	-63±16	1575	6.1±1.3 ₂₀	8.2±0.8	3.6±0.8	1522
	L	-144.3±5.2 ₁₂	-12.9±3.1	-24.8±3.1	1692	8.3±4.3 ₁₂	9.8±2.6	5.2±2.6	1693
A4	γ'	-200.2±11 ₁₂	-41.2±6.9	-53±6.9	1587	6.4±1.2 ₂₄	8.6±0.8	3.0±0.8	1512
	L	-172±56 ₄	-24±34	-36±34	1666	8.9±25 ₄	10.5±15	5.0±15	1666
B1	$\gamma'+\beta$	-88.2±3.9 ₁₈	10.7±2.6	-0.1±2.6	1544	-39.5±3.0 ₁₉	-18.9±1.9	-21.8±1.9	1544
	L	-141.0±3.9 ₆	-24.4±2.3	-35.3±2.3	1684	-8.4±5.1 ₆	1.1±3.0	-1.7±3.0	1684
B2	γ'	-146.5±6.8 ₂₁	-23.1±4.4	-34.2±4.4	1554	-10.5±1.4 ₂₉	-0.56±0.9	-4.3±0.9	1505
	L	-133.1±3.0 ₁₄	-14.7±1.8	-25.8±1.8	1693	6.2±3.1 ₁₄	9.3±1.8	5.6±1.8	1693
B3	γ'	-162.7±12.1 ₁₈	-30.3±7.8	-41.2±7.8	1562	-7.8±5.5 ₂₅	1.7±3.7	-3.3±3.7	1537
	L	-135.6±4.9 ₁₄	-12.4±2.9	-23.3±2.9	1688	6.9±4.3 ₁₄	10.0±2.6	5.0±2.6	1688
B4	γ'	-157.9±11.0 ₁₂	-21.6±7.0	-32.6±7.0	1560	-8.1±1.4 ₂₀	1.7±0.9	-4.4±2.6	1505
	L	-151.7±9.7 ₆	-16.5±5.8	-27.5±5.8	1684	5.3±5.7 ₆	9.6±3.4	3.5±3.4	1684

Note: subscript indicates the number of data points

Table 5. Proposed Solid ↔ Liquid Phase Transformations

Alloy	Proposed Phase Transformation	T range (K)
A1	$\gamma' + \text{Al}_2\text{O}_3 = \text{L} + \text{Al}_2\text{O}_3$	1620-1651
A2	$\gamma' + \text{Al}_2\text{O}_3 = \text{L} + \text{Al}_2\text{O}_3$	1627-1653
A3	$\gamma' + \text{Al}_2\text{O}_3 = \text{L} + \text{Al}_2\text{O}_3$	1620-1635
A4	$\gamma' + \text{Al}_2\text{O}_3 = \text{L} + \text{Al}_2\text{O}_3$	1623-1652
B1	$\gamma' + \beta + \text{Al}_2\text{O}_3 = \text{L} + \text{Al}_2\text{O}_3$	1637±5
B2	$\gamma' + \text{Al}_2\text{O}_3 = \gamma' + \text{L} + \text{Al}_2\text{O}_3 = \text{L} + \text{Al}_2\text{O}_3$	1620-1635
B3	$\gamma' + \text{Al}_2\text{O}_3 = \gamma' + \text{L} + \text{Al}_2\text{O}_3 = \text{L} + \text{Al}_2\text{O}_3$	1624-1637
B4	$\gamma' + \text{Al}_2\text{O}_3 = \gamma' + \text{L} + \text{Al}_2\text{O}_3 = \text{L} + \text{Al}_2\text{O}_3$	1620-1647

Figures

Figure 1. Ni-rich corner of the measured Ni-Al-Pt phase diagram at 1150°C (1423K) [1] showing the composition of the alloys measured in this study.

Note: Fig 1 needs to be shown beside Table 1.

Figure 2. Schematic of the Al_2O_3 effusion-cells used in this study: internal cell dimensions, 10mm in diameter by 7.5mm in height; effusion orifice 1.5mm in diameter by 4mm long. The orifice is offset by 2mm from cell centerline of the cell while the hole in the bottom is part of black-body source (2.5mm in diameter by 13.5mm deep).

Figure 3. Measured relative partial pressures of Au(g), Ni(g) and Al(g) and $\text{Al}_2\text{O}(g)$, $I_i T$, plotted as the natural logarithm versus inverse absolute temperature, $1/T$, from the activity measurement of alloys A2, Ni-24.2Al-10.0Pt, (Δ) and A4, Ni-23.8Al-25.1Pt, (\circ). The numbers on the Au(g) curve represent the order the measurements were made, each data point consists of 2 sets of 6 independent measurements taken 30–45 minutes apart. The measured relative partial pressure of Ni(g) in equilibrium with alloys A2 and A4 were identical and fall a single curve.

Figure 4. Measured $a(\text{Al})$ in γ' -(Ni,Pt)₃Al and liquid for alloys: A1, Ni-24.3Al-2Pt, (\diamond); A2, Ni-24.2Al-10Pt, (Δ); A3, Ni-24Al-18.1Pt, (\square); and A4, Ni-23.8Al-25.1Pt, (\circ). The results are plotted as the logarithm of $a(\text{Al})$ versus inverse absolute temperature, $1/T$.

Figure 5. Measured $a(\text{Ni})$ in $\gamma'-(\text{Ni,Pt})_3\text{Al}$ and liquid for alloys A1, Ni-24.3Al-2Pt, (\diamond); A2, Ni-24.2Al-10Pt, (\triangle); A3, Ni-24Al-18.1Pt, (\square); and A4, Ni-23.8Al-25.1Pt, (\circ). The results are plotted as the logarithm of $a(\text{Ni})$ verses inverse absolute temperature, $1/T$.

Figure 6. Measured $a(\text{Al})$ in $\gamma'-(\text{Ni,Pt})_3\text{Al}$ and liquid for alloys: B1, Ni-27.2Al-2Pt, (\diamond); B2, Ni-26.4Al-9.8Pt, (\triangle); B3, Ni-27Al-18.1Pt, (\square); and B4, Ni-26.7Al-25.2Pt, (\circ). The results are plotted as the logarithm of $a(\text{Al})$ verses inverse absolute temperature, $1/T$.

Figure 7. Measured $a(\text{Ni})$ in $\gamma'-(\text{Ni,Pt})_3\text{Al}$ and liquid for alloys: B1, Ni-27.2Al-2Pt, (\diamond); B2, Ni-26.4Al-9.8Pt, (\triangle); B3, Ni-27Al-18.1Pt, (\square); and B4, Ni-26.7Al-25.2Pt, (\circ). The results are plotted as the logarithm of $a(\text{Ni})$ verses inverse absolute temperature, $1/T$.

Figure 8. A plot of the measured partial entropies of mixing, $\Delta_m \bar{S}(i)$, for Al and Ni verses absolute T , for series A alloys.

Figure 9. A plot of the measured partial entropies of mixing, $\Delta_m \bar{S}(i)$, for Al and Ni verses absolute T , for series B alloys. Alloy B1 was not included here because it is not a single-phase $\gamma'-(\text{Ni,Pt})_3\text{Al}$ alloy.

Figure 10. SEM images of the surface of alloy B3: a) 250x image of the clean metallic surface of a dendrite with atomically flat steps, b) a composite image at 250x and 1000x of a region with fine crystalline Al_2O_3 precipitates in a clean metallic surface.

Figure 11. The excess mixing behavior of Ni in $\gamma'-(\text{Ni,Pt})_3\text{Al}$ and liquid plotted as the logarithm of γ_{Ni} verses inverse absolute temperature, $1/T$: a) series A alloys and b) series B alloys.

Figures

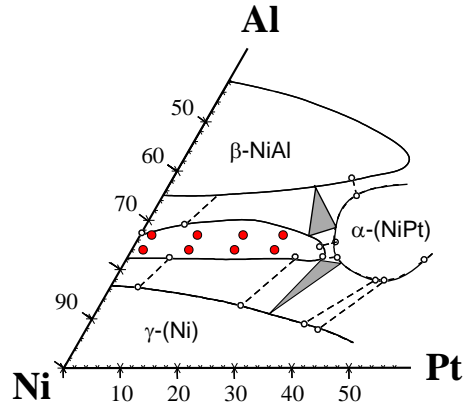


Figure 1. Ni-rich corner of the measured Ni-Al-Pt phase diagram at 1150°C (1423K) [1] showing the composition of the alloys measured in this study.

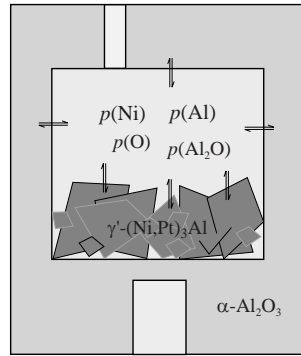


Figure 2. Schematic of the Al_2O_3 effusion-cells used in this study: internal cell dimensions, 10mm in diameter by 7.5mm in height; effusion orifice 1.5mm in diameter by 4mm long. The orifice offset by 2mm from cell centerline of the cell while the hole in the bottom is part of black-body source (2.5mm in diameter by 13.5mm deep).

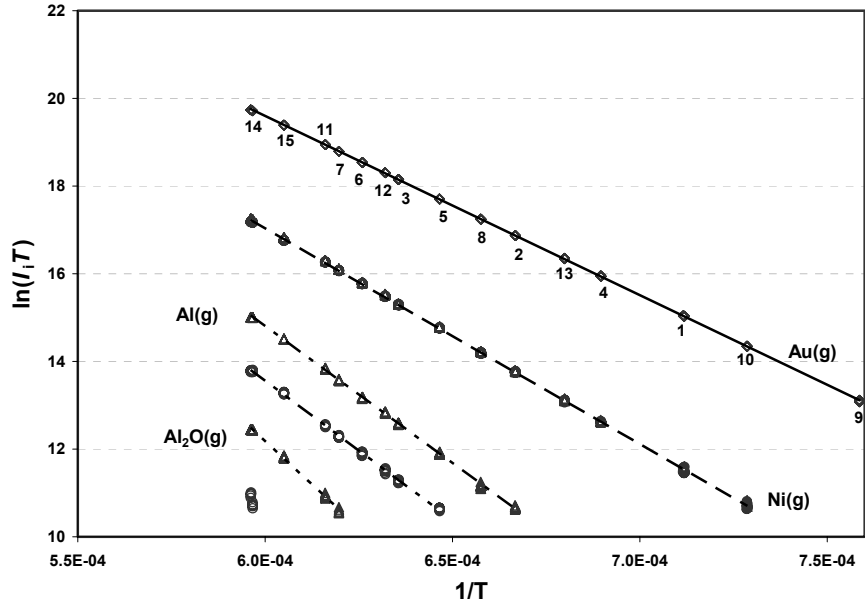


Figure 3. Measured relative partial pressures of Au(g), Ni(g) and Al(g) and Al₂O(g) plotted as the natural logarithm versus inverse absolute temperature, $1/T$, from the activity measurement of alloys A2, Ni-24.2Al-10.0Pt, (Δ) and A4, Ni-23.8Al-25.1Pt, (\circ). The numbers on the Au(g) curve represent the order in which the measurements were made, each data point consists of two sets of 6 independent measurements taken 30–45 minutes apart. The measured relative partial pressure of Ni(g) in equilibrium with alloys A2 and A4 were identical and fall a single curve.

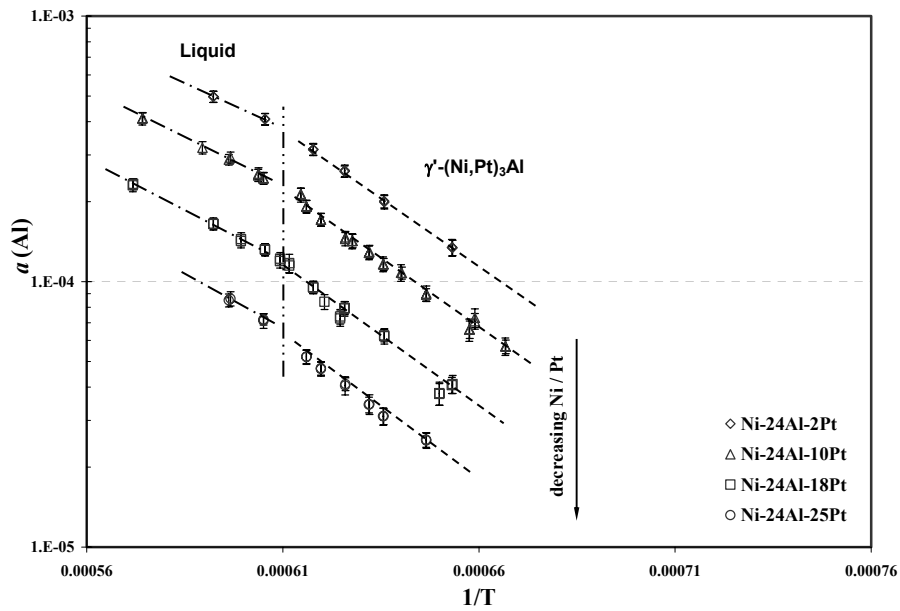


Figure 4. Measured $a(\text{Al})$ in $\gamma'-(\text{Ni,Pt})_3\text{Al}$ and liquid for alloys: A1, Ni-24.3Al-2Pt, (\diamond); A2, Ni-24.2Al-10Pt, (Δ); A3, Ni-24Al-18.1Pt, (\square); and A4, Ni-23.8Al-25.1Pt, (\circ). The results are plotted as the logarithm of $a(\text{Al})$ versus inverse absolute temperature, $1/T$.

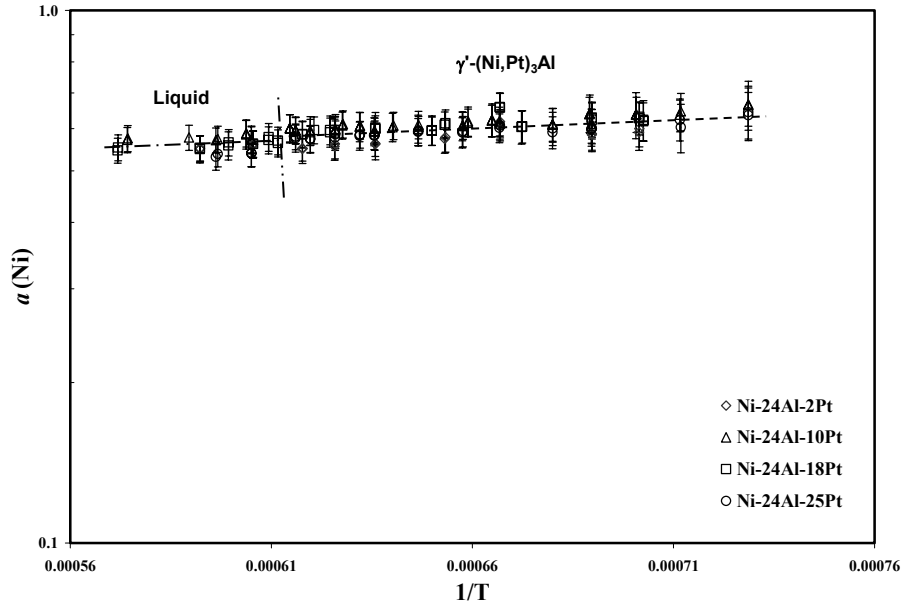


Figure 5. Measured $a(\text{Ni})$ in $\gamma'-(\text{Ni,Pt})_3\text{Al}$ and liquid for alloys A1, Ni-24.3Al-2Pt, (\diamond); A2, Ni-24.2Al-10Pt, (\triangle); A3, Ni-24Al-18.1Pt, (\square); and A4, Ni-23.8Al-25.1Pt, (\circ). The results are plotted as the logarithm of $a(\text{Ni})$ versus inverse absolute temperature, $1/T$.

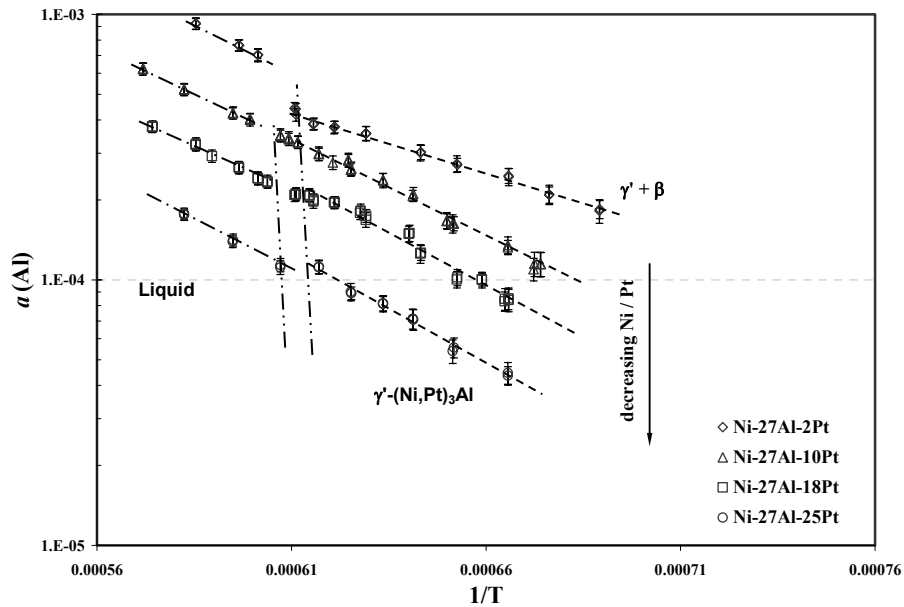


Figure 6. Measured $a(\text{Al})$ in $\gamma'-(\text{Ni,Pt})_3\text{Al}$ and liquid for alloys: B1, Ni-27.2Al-2Pt, (\diamond); B2, Ni-26.4Al-9.8Pt, (\triangle); B3, Ni-27Al-18.1Pt, (\square); and B4, Ni-26.7Al-25.2Pt, (\circ). The results are plotted as the logarithm of $a(\text{Al})$ versus inverse absolute temperature, $1/T$.

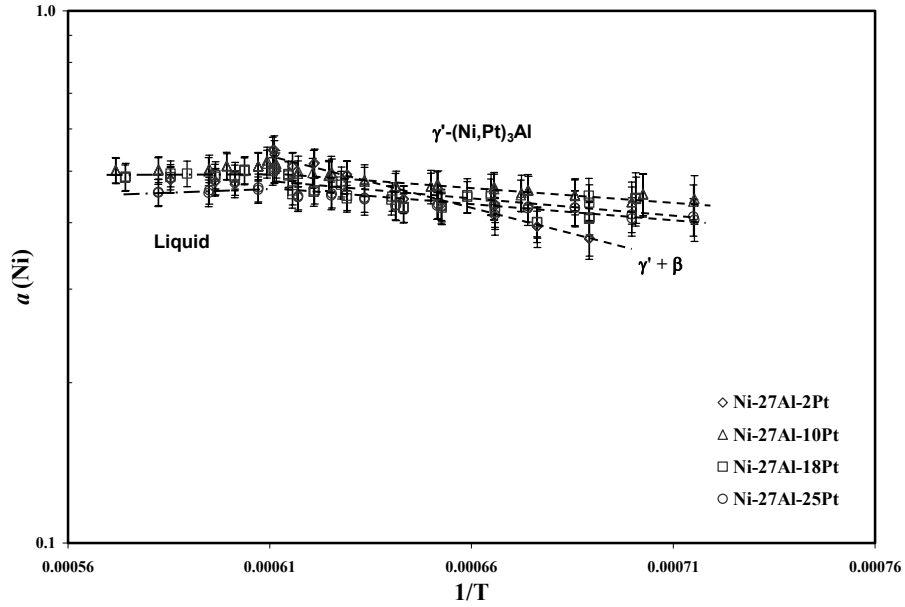


Figure 7. Measured $a(\text{Ni})$ in $\gamma'-(\text{Ni,Pt})_3\text{Al}$ and liquid for alloys: B1, Ni-27.2Al-2Pt, (\diamond); B2, Ni-26.4Al-9.8Pt, (\triangle); B3, Ni-27Al-18.1Pt, (\square); and B4, Ni-26.7Al-25.2Pt, (\circ). The results are plotted as the logarithm of $a(\text{Ni})$ versus inverse absolute temperature, $1/T$.

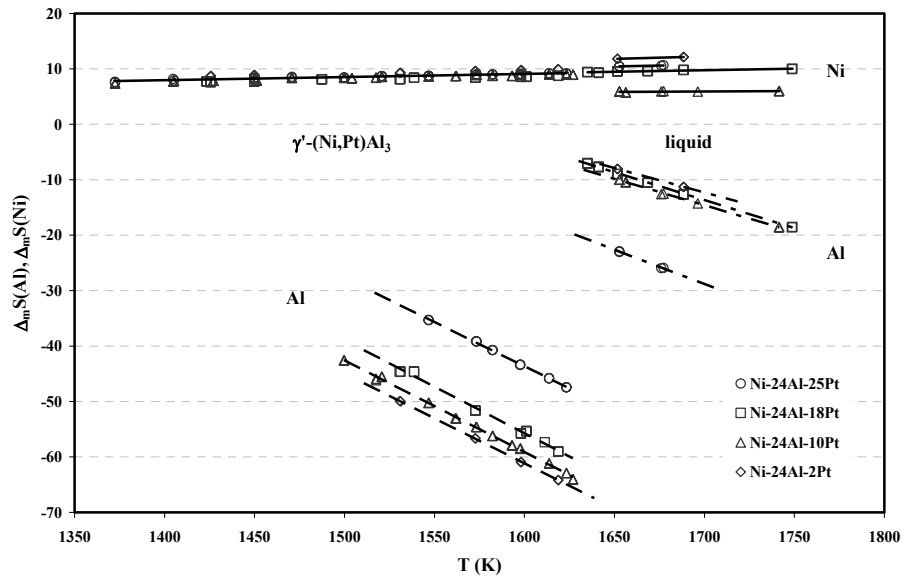


Figure 8. A plot of the measured partial entropies of mixing, $\Delta_m \bar{S}(i)$, for Al and Ni versus absolute T , for series A alloys.

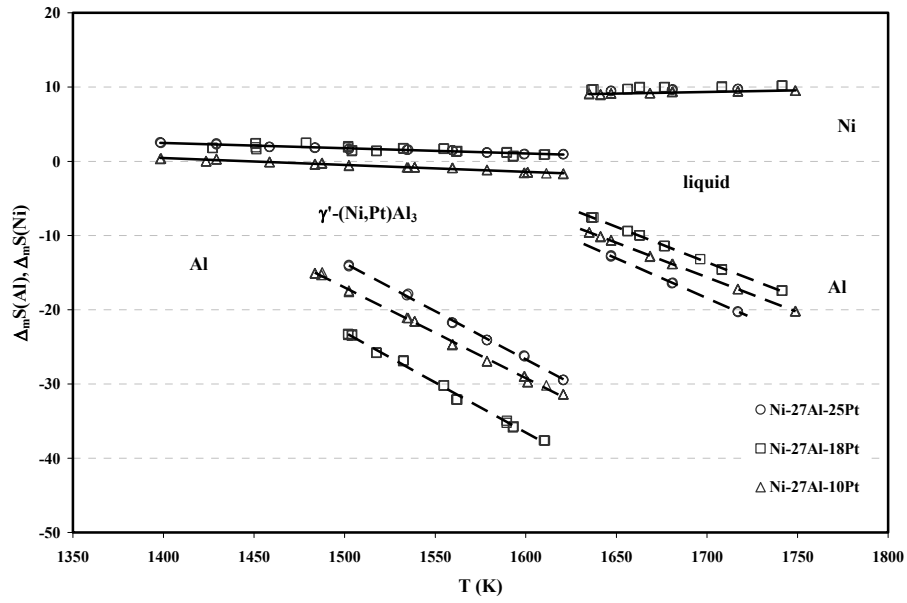


Figure 9. A plot of the measured partial entropies of mixing, $\Delta_m \bar{S}(i)$, for Al and Ni versus absolute T , for series B alloys. Alloy B1 was not included here because it is not a single-phase $\gamma'-(Ni,Pt)_3Al$ alloy.

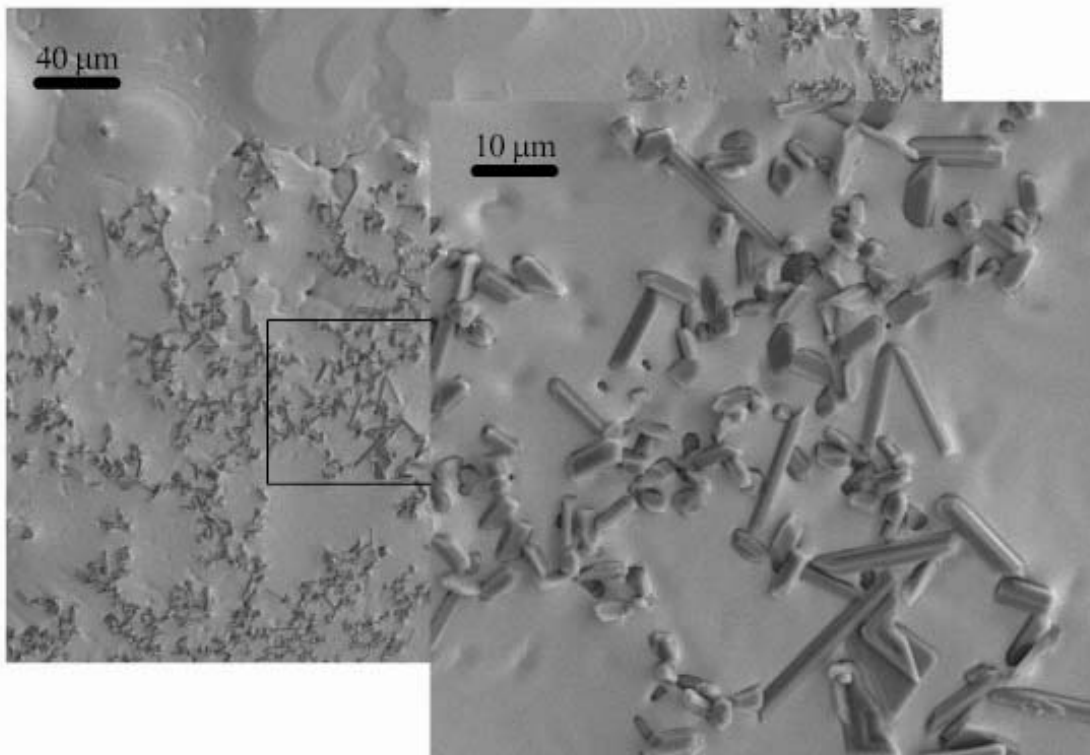
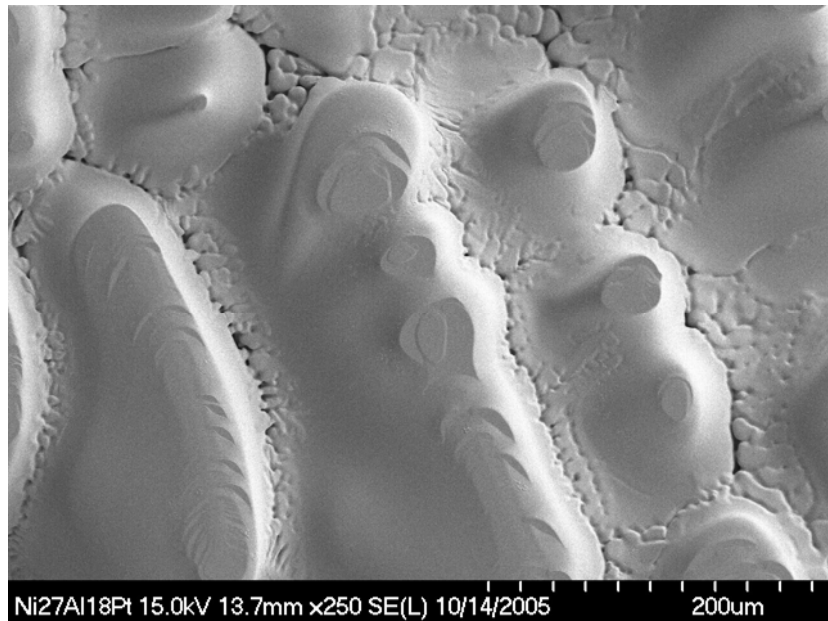


Figure 10. SEM images of the surface of alloy B3: a) 250x image of the clean metallic surface of a dendrite with atomically flat steps, b) a composite 250x and 1000x image a region with fine crystalline Al₂O₃ precipitates in a clean metallic surface.